JOINT EUROPEAN TORUS

JET–P(89)12

J.P. Christiansen, J.G. Cordey, D. Muir
and JET Team

Local Transport in Sawtooth-Free JET Discharge

Local Transport in Sawtooth-Free JET Discharge

J.P. Christiansen, J.G. Cordey, D. Muir
and JET Team*

JET-Joint Undertaking, Culham Science Centre, OX14 3DB, Abingdon, UK

** See Appendix 1*

Preprint of Paper to be submitted for publication in
Nuclear Fusion

Local Transport in Sawtooth-free JET Discharges

J P Christiansen, J G Cordey, D Muir
JET Joint Undertaking, Abingdon, Oxon, OX14 3EA

ABSTRACT

Application of ICRH to the central region of the plasma can produce sawtooth-free periods of duration several confinement times and central electron temperatures in excess of 10keV. The resulting electron transport is studied locally by examining the relationship between total heat flux and temperature and density gradients. The spatial profile of heat diffusivity is found to be virtually independent of plasma current in the central region and strongly dependent upon current in the outer region. When this result is combined with those obtained from respectively RF modulation experiments, heat pulse propagation measurements and transient plasma responses from pellet injection, a coherent picture of heat diffusivity profiles emerges: Together these results confirm that the global confinement time has a dependence upon plasma current which is weaker than linear.

1. INTRODUCTION

The problems associated with determining local plasma transport properties from experimental measurements are well known. References [1-3] describe local transport studies carried out on the TFTR, D-IIID and JET tokamaks. The aims of such studies are: 1) to estimate values of the local heat diffusivity χ either for electrons or for ions or for both and 2) to establish the dependence (scaling) of χ with basic plasma parameters like density, temperature, etc. Presently no general scaling law for χ has emerged to explain the wealth of diagnostic measurements from the above-mentioned large tokamaks; these measurements include time-dependent spatially resolved profiles of electron temperature and density and sometimes ion temperature profiles as well. Sources of errors from time-space differences of experimental measurements together with sawteeth effects, non-steady states, etc combine to produce plenty of scope in the interpretation of χ scaling studies. The work to be described in this paper does not provide for a full solution to these problems; it eliminates however, the effects of sawteeth, effects which increase the scatter in the data such as that of reference [3].

Discharges with sawtooth-free periods lasting several confinement times are produced in JET by application of ICRH with a frequency corresponding to the central plasma region [4]. These discharges, sometimes referred to as discharges with "monster sawteeth", have been produced regularly in ICRH experiments. Despite its name ICRH mainly heats the electrons since the minority ions (He^3 or H) slow down from energies above 1MeV via electron friction. In some discharges the electrons become decoupled from the ions in the sense that the equipartition time τ_{eq} exceeds the electron energy confinement time τ_{Ee} by a factor 1 to 2. Fig. 1 shows the time evolution of the central electron temperature T_e during the application of 10MW of ICRH in JET pulse #13428. This pulse is one out of 110 pulses with sawtooth-free periods which have been used in the present study. The cause of and termination of the sawtooth-free period is presently not understood; for the case shown in Fig. 1 it happens before the end of the ICRH and $T_e(0)$ drops 4keV, only to rise 4keV again for a short period. The arrows in Fig. 1 indicate the many time values used in the analysis of that pulse.

The transport analysis method used is similar to that used in reference [3]. It will be described briefly in Section 3 together with the criteria adopted for data selection. The next Section 2 presents some of the characteristics of the JET sawtooth-free discharges. The data set used in the analysis is surveyed in Section 4 and we emphasise which variables are dependent and which are independent ones. Section 5 examines the "raw" data and the role of energy equipartition. The results deduced from the analysis yield the spatially resolved profile of heat diffusivity χ; the scaling of χ is attempted in Section 6 by fits of the experimental data to an empirical and to a theoretical model. The results are complemented by values of χ obtained from different analysis methods. The first method models, via a simple diffusion equation, the modulation response of the axial value T_e to modulation of the ICRH power [5]. The second method is based on heat pulse propagation studies [6] of other JET discharges with similar parameters; the sawtooth-free discharges produce a heat pulse only at the termination of the "monster sawtooth".

The main result of our analysis is a plasma current dependence of χ in the outer region as found in [3], but no detectable dependence of χ upon current or any other parameters in the inner region. Section 7 discusses possible interpretations of this result by correlating it to the results obtained by other analysis methods.

2. CHARACTERISTICS OF SAWTOOTH-FREE DISCHARGES

In four series of experiments involving 110 ICRH plasma discharges, the toroidal components of plasma current I_ϕ and field B_ϕ are varied as follows:

$$(I_\phi, B_\phi) \sim (2,2)\ ,\ (2.5, 2.5)\ ,\ (3,3) \text{ and } (3.5, 3.5) \qquad (1)$$

the units being MA and Tesla. For each series (I_ϕ, B_ϕ) of experiments the ICRH power varies from 3 to 13MW and all discharges have centrally peaked power deposition profiles. Each discharge exhibits one (sometimes two or three) sawtooth-free period whose duration can vary from 0.5 to 3 seconds [4].

The plasma configuration is an elliptic cross-section, ellipticity 1.5, attached to the JET belt limiter. This means that the spatial profile of the safety factor $q_\psi(x)$ is essentially the same for all discharges; x is a normalised radius or flux surface label $0 \leq x \leq 1$. Fig. 2 shows four such q_ψ profiles, one from each of the series (1); these profiles are obtained from calculations with the equilibrium code IDENTC [7] in which the current distribution is estimated by fits to magnetic measurements.

The global plasma confinement exhibits a dependence upon plasma current I_ϕ. Fig. 3 shows the total electron energy W_e against $P - \frac{dW_e}{dt}$; W_e is evaluated from temperature profiles (ECE) and density profiles (interferometer) and P denotes total input power. The four different symbols used throughout all the Figures in this paper, label the four values of I_ϕ; the data clearly separate into four groups of points. The offset-linear scaling law often used to represent the total energy (thermal + fast ions) [8,9] is a good representation of the W_e data in Fig. 3, ie,

$$W_e = W_e(0) + \tau_{einc}\ (P - \frac{dW_e}{dt}) \quad . \qquad (2)$$

Both the offset $W_e(0)$ and the incremental electron confinement time depend on plasma current.

The energy content of fast minority ions can be estimated because it is predominantly anisotropic, ie, $W_{fast} = W_{\perp fast}$. It can be shown [10]

$$W_{\perp fast} = \frac{4}{3} (W_{dia} - W_{MHD}) = \frac{2}{3} (W_{dia} - W_{kin}) \quad . \tag{3}$$

In (3) W_{dia}, W_{MHD} and W_{kin} denote respectively the total perpendicular energy (diamagnetic loop), the energy from MHD fits [7,11] and the total thermal energy; in the latter similar electron and ion temperature profiles are assumed . If the fast ion energy content reaches a steady state it should equal $P_{RF}\ \tau_s/2$ where P_{RF} is total ICRH power and τ_s is the characteristic slowing down time [12]

$$\tau_s \approx 0.11 \frac{T_e^{3/2}}{n_e} \frac{A_f}{Z_f^2} \quad . \tag{4}$$

A_f, Z_f are the atomic mass and charge numbers of the minority ion and the units in (4) for T_e and n_e are keV and $10^{19} m^{-3}$. Fig. 4 shows the fast ion energy estimate given by (3) plotted against $P_{RF}\ \tau_s/2$; the symbols in Fig. 4 again label the plasma current. For the 2, 2.5 and 3MA data there is a clear correlation between measured and theoretical estimates of $W_{\perp fast}$ which represents up to 25% of the total energy W_{dia}. All experiments at 2, 2.5 and 3MA have He^3 as majority ions and H as minority ions. In the 3.5MA, 3.5 Tesla experiments, on the other hand, He^4 is the majority ion and He^3 the minority ion. Both estimates of $W_{\perp fast}$ given by (3) show a systematic offset arising from errors in W_{dia} at 3.5MA.

3. HEAT FLUX DUE TO ICRH

The transport analysis is based on the prescription given in [13] and used previously for JET NBI heated discharges [3]. Two improvements over the previous studies are the absence of sawteeth and the inclusion of radiation profiles. Both improvements lead to a significant reduction in the scatter of the data on q(x), the total heat flux. The latter is calculated from

$$q(x) = \frac{1}{a \langle |\nabla x|^2 \rangle V'} \int_0^x (Q_{ICRH} + Q_\Omega - Q_R - \frac{dW}{dt}) V' dx \quad . \tag{5}$$

The minor radius is a, V′ denotes d/dx of volume. The source terms are calculated as follows. Q_Ω is derived by the method of [3] and Q_R by Abel inversion of bolometer data. The volume integral P_{RF} of Q_{ICRH} is derived from the theoretical prediction of [14]. For each plasma surface x the following approximation is made.

$$P_{RF}(x) = P_{TOTAL}(\alpha,\ P_1(x) + (1-\alpha)P_2(x)) \tag{6}$$

$P_1(x)$ denotes the volume integrated deposition in large aspect ratio, circular flux surface geometry

$$P_1(x) = (1-2\ \exp(-(\frac{x}{S_0})^2))/(1-2\ \exp(-\frac{1}{S_0^2})) \tag{7}$$

where the half-width of the resonance layer S_0 is approximated by

$$S_0 = 0.538d + 0.087 \quad . \tag{8}$$

The Doppler broadening parameter d is

$$d = \frac{n}{a\omega}\ V_{th}(\text{minority}) \quad , \tag{9}$$

where n is a toroidal mode number (10 for monopole, 25 for dipole antenna configurations), ω the ICRF and V_{th} the minority thermal velocity. The weak damping power integral is approximated as in [14]

$$P_2(x) = \int_0^x f(x)n_i(x)dx / \int_0^1 f(x)n_i(x)dx \quad . \tag{10}$$

To evaluate (10) f(x) is taken from Fig. 5 of [14].

Finally the damping coefficient α is estimated from [14] and is of order 0.2. An example of the spatial variation of the calculated q(x) profiles is presented in Fig. 5 for the same pulse whose electron temperature is shown in Fig. 1; the three profiles of Fig. 5 labelled 1 to 3 are calculated at the times so labelled in Fig. 1.

The ICRF power and thus the flux q(x) have been varied independently of field, plasma current and density. Such a variation is the basic ingredient for the transport analysis method which examines the relationship

$$q = - \chi \, e n_e \langle \nabla T_e \rangle - q_{pinch} \qquad (11)$$

by comparing calculated local values of q(x) with measurements of $n_e(x)$ and the surface average at x of ∇T_e. In Eq.(11) the local heat diffusivity χ may depend on local plasma parameters such as temperature or density; χ may also depend on gradients, eg, $\langle \nabla T_e \rangle$. The heat flow or heat pinch term q_{pinch} will not be restricted to any specific form, however, it is in general difficult to determine. The data set selected includes 820 observations from 110 pulses. The selection excludes by the restriction

$$0 < \frac{1}{P_{TOTAL}} \frac{dW}{dt} < 0.4 \qquad (12)$$

strong non-steady states, in particular those close to sawtooth collapses. From this data we further select values at only 3 radial positions [3], x = ½, ²/₃, ¾. The reason for this choice is that Eq.(6) for ICRH deposition is only approximate for x < ½; for x > ¾ the radiation profile $Q_R(x)$ is similarly only approximately known.

4. INNER RELATIONS IN DATA

Figure 2 illustrate that the values of safety factor q_ψ at x = ½, ²/₃, ¾ are respectively 1.4, 1.9, 2.3 with little variation within the groups of pulses (1). A similar lack of variation is found in the normalised spatial profiles

$$\lambda_T = \frac{\langle \nabla T_e \rangle}{T_e} \quad , \quad \lambda_n = \frac{\langle \nabla n_e \rangle}{n_e} \quad . \qquad (13)$$

For each of the groups of pulses (1) λ_T and λ_n are approximately constant at a given x. The variation of λ_T and λ_n with plasma current is more pronounced at x = ½ than at x = ¾.

$$\begin{aligned} &2MA \quad : \lambda_T\,(½) \approx 2.2 \;, \quad \lambda_T\,(¾) \approx 2.7 \;, \\ &3.5MA \; : \lambda_T\,(½) \approx 1.4 \;, \quad \lambda_T\,(¾) \approx 2.4 \;, \end{aligned}$$

ie, the 2MA profiles are more peaked than those at 3.5MA. Within each group of pulses (1) it is therefore difficult to distinguish between a dependence of q or χ (Eq.11) upon T_e or upon $\langle \nabla T_e \rangle$. The same argument applies to n_e and $\langle \nabla n_e \rangle$. The changes to the profiles (13) caused by changes in q (ICRH power) or changes in I_ϕ can be studied in plots of η_e vs q at a given x, or η_e (x = ½) vs η_e (x = ¾) etc, where η_e is defined as

$$\eta_e = \frac{\lambda_T}{\lambda_n} = \frac{\partial \log T_e}{\partial \log n_e} \quad . \tag{14}$$

At the half radius ($x = \frac{1}{2}$) η_e is found to vary weakly with q and strongly with I_ϕ. For $x = \frac{3}{4}$ the η_e data scatters around $\eta_e = 2$ with no q or I_ϕ dependence.

The variations of q(x) have been made experimentally almost independently of the plasma density n_e. Thus the $\langle \nabla T_e \rangle$ values resulting from ICRH and the corresponding values of n_e are almost independent of each other; plots of $\langle \nabla T_e \rangle$ vs n_e similar to Fig. 4 of reference [3] verify such a data independence.

5. RAW DATA AND EQUIPARTITION

The heat flux method examines if the relationship (11) can represent the data of calculated values of q and measured values of n_e and $\langle \nabla T_e \rangle$. The assumptions which may make Eq.(11) a useful representation of total heat flow in an axisymmetric tokamak (no sawteeth effects) are as follows:

1. The major part of the heat flow is through the electron thermal loss channel.

2. The electron and ion thermal diffusivities χ_e and χ_i are for $x > 0.5$ not too dissimilar in magnitude and in their scaling with plasma parameters.

A consequence of these assumptions is that ion-electron energy equipartition rate Q_{ei} does not play a dominant role in the heat flow such that terms proportional to $\langle \nabla T_i \rangle$ would be required in Eq.(11). To assess if this is the case we evaluate

$$Q_{ei} = \frac{3}{2} n_e e \frac{T_e - T_i}{\tau_{eq}} \tag{15}$$

in which the equipartition time is $\tau_{eq} = \tau_s(A_f=3, Z_f=2)/Z_{eff}$; τ_s is given by Eq.(4). By replacing the integrand in Eq.(5) with Q_{ei} we can calculate the flux q_{ei} associated with equipartition and estimate its magnitude in the equation

$$q = q_e - q_{ei} \quad ,$$

in which q_e denotes the electron heat flux. The calculation requires an ion temperature profile and we assume

$$T_i(x) = (T_{io} - T_e(x = 1))(1 - x^2)^\gamma + T_e(x = 1) \ , \qquad (16)$$

where T_{io} is measured by the JET X-ray crystal spectrometer.

By varying γ we find that q/q_{ei} is at most 10-12% (2MA) and 6-7% (3.5MA); these values are for $\gamma = 3$, a rather peaked $T_i(x)$ profile. By further increases to γ the ratio q_{ei}/q will increase further; it appears however unlikely that the ion temperature profile $T_i(x)$ should become more peaked during the ICRH than during the ohmic phase. A 6 to 10% change to the heat flux q due to ion-electron equipartition indicates that the electron energy loss channel is indeed the dominant one and χ in Eq.(11) should be close to the electron thermal diffusivity χ_e.

Before proceeding to fit the data to Eq.(11) we first examine the "raw" data. Figs. 6 and 7 show values at $x = \frac{1}{2}$ and $\frac{3}{4}$ respectively of q plotted against values of the product $en_e\langle\nabla T_e\rangle$ (the electron charge e is used as T_e is in units eV). We have only included the 2 and 3.5MA data to bring out the following point: at $x = \frac{1}{2}$ there is little dependence of the slope $dq/d(en_e\langle\nabla T_e\rangle)$ upon current; at $x = \frac{3}{4}$ there is a pronounced dependence upon current. The lines through the data points arise from linear regression fits to these and their slope represent an ensemble averaged $\tilde{\chi}$. The intercept at $en_e \nabla T_e = 0$, ie, q_{pinch} of Eq.(11), is almost zero at $x=\frac{1}{2}$ (Fig. 6). As x increases q_{pinch} increases and Fig. 7 shows a finite q_{pinch} for both the 2 and 3.5MA data.

6. SCALING LAWS FOR HEAT DIFFUSIVITY

Two scaling laws for the total diffusivity χ are used to fit the data to the expression (11). The first scaling law involves an empirical dependence of χ upon those parameters which we regard as being varied independently in the data set:

$$\chi_1 = K\, n_e^a\, T_e^b\, I_\phi^c \quad . \qquad (17)$$

We note following Section 4 that $\langle \nabla n_e \rangle$ and $\langle \nabla T_e \rangle$ could replace n_e and T_e respectively in Eq.(17). The second scaling law is based on the work of Connor [15]. The scale invariance technique of Connor-Taylor [16] has been applied by Hagan and Frieman [17] to a non-linear gyrokinetic equation. The technique yields the general expression

$$\chi_2 = K \frac{\rho^2 v}{L} \; F\left(\frac{\nu L}{v}, \beta\right) , \tag{18a}$$

in which ρ is Larmor radius (electrons or ions), v is thermal velocity (e or i), L a scale length, ν a collision frequency and β denotes plasma β (toroidal or poloidal). The expression (18a) is rather general and permits vast number of possible scalings through permutations of variables, eg, ρ_e, ρ_i, v_e, v_i, etc. We have used a power series representation of (18a) which takes the form

$$\chi_2 = K \frac{T_e^{3/2}}{I_\phi^2 L} \left(\frac{n_e L}{T_e}\right)^a \left(\frac{n_e T_e}{I_\phi^2}\right)^b . \tag{18b}$$

For the JET data represented by the groups (1) it is clear that any I_ϕ dependence of χ can be interpreted as a B_ϕ dependence.

We carry out non-linear regression fits of the data to Eq.(11) using the expressions (17) and (18b). Tables I and II summarise the values of the parameters K, a, b, c obtained by fits to data at a fixed x and fits to all the data. Both the χ_1 and χ_2 scaling confirm that the heat pinch q_{pinch} is small; this is already evident from Figs. 6 and 7. Fitting the data on heat flux q to Eq.(11), using either Eq.(17) or (18b) for χ and allowing for some specific form of the heat pinch q_{pinch}, is difficult. The scatter in the data on q is of the same magnitude as the inferred q_{pinch} which is treated as a constant. The parameter values in tables I and II show that the non-linear regression analysis may yield either positive or negative values of q_{pinch} depending on the choice of χ and on the radial coordinate. Both scalings show nevertheless that there is a strong current dependence at x = ¾, a weaker one at x = ²/₃ and hardly any I_ϕ dependence at x = ½. If all x values are combined then the current dependence of χ becomes small because the weight in the fitting of the x = ½ and ²/₃ exceeds by a factor 2 that of the x = ¾ data. Presently we can therefore not exclude any "hidden variables" in either the χ or q_{pinch} scaling. When introduced, such variables would permit an arbitrary selection of data at various radial positions to be made and used in non-linear regression fits.

7. INTERPRETATION OF RESULTS

The resulting heat diffusivity profile $\chi(x)$ is shown in Fig. 8 for plasma currents of 2 to 3.5MA. Also shown in Fig. 8 is the value of χ with error bars deduced from ICRH modulation experiments [5] during sawtooth-free discharges; this value applies to the centre of the discharge and has been obtained in separate experiments with I_ϕ = 2MA, but B_ϕ = 3.4T. A second value for χ_e has been found [18] with 3MA, 3T confirming that there is no variation with plasma current.
The heat pulse propagation method for estimating χ_{HP} [6] has been applied to plasma configurations with an internal separatrix. In the discharges at I_ϕ = 3, 3.5 and 4MA sawteeth are produced by NBI heating. The range of values χ_{HP} from the analysis [19] are represented by an error bar in Fig. 8 at a range in radius $0.4 < x < 0.6$ just outside the sawtooth inversion radius. The data in [19] show no systematic dependence of χ_{HP} upon I_ϕ.

A fourth method [20] has been used to estimate χ_e. It is based on analysis of the transient plasma response generated by pellet injection into NBI heated plasmas with I_ϕ = 3MA and B_ϕ = 3T. Fig. 8 shows the values of χ_e for two pulses at 2 and 3MA and these are marked by horizontal error bars.

The results in Fig. 8 for χ, χ_e, χ_{HP} obtained from data of different types of experiments by different analysis methods and at various spatial locations in the plasma summarise the first statement of this paper. For sawtooth-free discharges there is no apparent dependence of χ_e upon plasma current or field inside the $x = {}^1/_2$ radius. For sawteething discharges a slightly higher χ_e is deduced in this region, but again without any obvious current dependence. At the ¾ radius the result from this paper can be expressed approximately as

$$\chi(x = \tfrac{3}{4}) \approx \frac{7.5}{I_\phi(\mathrm{MA})} \quad [\mathrm{m^2/s}]$$

in agreement with the estimate for NBI heated discharges [3] for which the scatter (mean rms of relative difference between data and fit) was 35%. The suppression of sawteeth has diminished the scatter (σ in tables I and II) to 22%; this represents a substantial improvement.

The heat diffusivity profiles which can be inferred from Fig. 8 indicate the variations of χ_e with x and I_ϕ (B_ϕ) that may be expected in ICRF heated plasmas which exhibit L-mode confinement. To correlate the profiles for local diffusivity with global confinement scaling (Fig. 3) it is necessary to evaluate the density-volume weighted average $\bar{\chi}$ defined in [13] as

$$\bar{\chi} = \left(4 \int_0^1 \frac{\int_0^x n_e(x') \sqrt{g}\, dx'}{a^2 E \langle|\nabla x|^2\rangle n_e(x) \sqrt{g}\, \chi(x)}\, dx\right)^{-1} . \qquad (19)$$

E denotes ellipticity and the volume element is $dv = \sqrt{g}\, dx$. Eq.(19) can be evaluated assuming [11,13]

$$n_e(x) = n_0 (1 - x^2)^\gamma$$
$$\chi(x) = \chi_0 / (1 - x^2)^\beta \quad . \qquad (20)$$

It can be inferred from the shape of the curves in Fig. 8 that β depends on current. The model profiles (20) are however too steep beyond say x=0.8, where no information on χ is available. We therefore replace the upper limit on the integral (19) by x=0.8 and we use $\beta = \frac{1}{2}(4 - I_\phi)$ to bring out the variation of χ with current. A fit to the 4 values of $\bar{\chi}$ thus obtained yields

$$\bar{\chi} = (4 \pm 0.07)\ I_\phi^{-0.5}\ (m^2/s)$$

with I_ϕ in units MA. The incremental confinement time τ_χ defined in [13] then becomes

$$\tau_\chi = \frac{3a^2E}{4\bar{\chi}} = 0.085\ I_\phi^{0.5}\ (s) \qquad (21)$$

Such a scaling has recently been inferred [9] from studies of sawtooth effects on confinement. The slopes of the global confinement data in Fig. 3 are represented by the expression for τ_χ as should be expected. The offset $W_e(0)$ in Eq.(2) is evident in the data of Fig. 3. This offset arises from the offset q_{pinch} and is derived in [13] as

$$W_e(0) = \tau_\chi \int_0^1 \frac{\int_0^x n_e(x')\sqrt{g}\, dx'}{a^3 E \langle|\nabla x|^2\rangle n_e(x)\, \chi/\bar{\chi}}\, q_{pinch}\, dx + W_1 \quad . \qquad (22)$$

In Eq.(22) W_1 represents a contribution from finite edge temperature; this contribution is small for the series of experiments studied in this paper. The variation of q_{pinch} with radius x and with plasma current I_ϕ is difficult to establish quantitatively; this is borne out by values in Tables I and II. Figs. 6 and 7 show, however, qualitatively that q_{pinch} increases with x and plasma current. If a radially increasing variation of q_{pinch} is assumed in Eq.(22) together with $\chi(x)$ as shown in Fig. 8 then we can qualitatively infer that the integral in Eq.(22) will exhibit the same current dependence, eg, $\sim I_\phi^\alpha$, $\alpha > 0$. The offset $W_e(0)$ will thus depend on I_ϕ more strongly than τ_χ. This dependence $W_e(0)$ vs I_ϕ is clearly shown in Fig. 3 and varies from 0.6MJ at 2MA to 1.1MJ at 3.5MA.

8. SHORT SUMMARY

The suppression of sawteeth by ICRH substantially improves the quality of the data used for the heat flux method to determine local transport. The results obtained with this method for 110 JET pulses have been combined with results from three other methods which estimate the diffusivity. Together they produce a coherent picture of the heat diffusivity profiles: the heat diffusivity inside the ½ radius shows little dependence upon plasma current; as x increases from ½ to 1 the dependence upon current becomes stronger.

When the diffusivity profiles are interpreted according to the method of [13], the experimentally observed dependence of global confinement upon plasma current is established.

ACKNOWLEDGEMENTS

The authors wish to thank K Thomsen for assistance with the work on the data bank and they wish to thank D J Campbell for producing a catalogue of sawtooth-free discharges. Discussions with J D Callen about scaling of χ and the role of equipartition are also acknowledged.

REFERENCES

[1] TANG, W.M., Nucl. Fusion 26 (1986) 1605.

[2] WALTZ, R.E., WONG, S.K., GREENE, J.M., DOMINGUEZ, R.R., Nucl. Fusion 26 (1986) 1729.

[3] CHRISTIANSEN, J.P., CALLEN, J.D., CORDEY, J.G., THOMSEN, K., Nucl. Fusion 28 (1988) 817.

[4] CAMPBELL, D.J., START, D.F.H., WESSON, J.A. et al., Phys. Rev. Lett. 60 (1988) 2148.

[5] START, D.F.H., BHATNAGAR, V.P., BOYD, D.A. et al., IAEA-CN-50/E-II-3, 12th IAEA Conf. on Plasma Physics and Controlled Nuclear Fusion (Nice, France) 1988.

[6] TUBBING, B.J.D., LOPEZ-CARDOZO, N.J., van der WIEL, M.J., Nucl. Fusion 27 (1987) 1843.

[7] BLUM, J., le FOLL, J., J. Comp. Phys. Rep. 1 (1984) 465.

[8] CORDEY, J.G., BARTLETT, D.V., BHATNAGAR, V.P. et al., IAEA-CN-47/A-II-3, 11th IAEA Conf. on Plasma Physics and Controlled Nuclear Fusion (Kyoto) 1986.

[9] BHATNAGAR, V.P., CAMPBELL, D.J., CHRISTIANSEN, J.P. et al., Effect of sawteeth and safety factor q on confinement during ICRF heating of JET, 15th EPS Conf. on Controlled Fusion and Plasma Heating (Dubrovnik) 1988.

[10] COOPER, W.A., WOOTTON, A., Plasma Physics 24 (1982) 1183.

[11] CHRISTIANSEN, J.P., J. Comp. Phys. 73 (1987) 85.

[12] STIX, T.H., Nucl. Fusion 15 (1975) 737.

[13] CALLEN, J.D., CHRISTIANSEN, J.P., CORDEY, J.G., THOMAS, P.R., THOMSEN, K., Nucl. Fusion 27 (1987) 1857.

[14] HELLSTEN, T., VILLARD, L., Nucl. Fusion 28 (1988) 285.

[15] CONNOR, J.W., Plasma Physics and Controlled Fusion 30 (1988) 619.

[16] CONNOR, J.W., TAYLOR, J.B., Nucl. Fusion 17 (1977) 1047.

[17] HAGAN, W.K., FRIEMAN, E.A., Phys. Fluids 29 (1986) 3635.

[18] START, D.F.H., ICRF power modulation experiments during monster sawteeth. To be published.

[19] de HAAS, J.C.M., LOPEZ-CARDOZO, N.J., Abstract 6U4, Bull. of the APS 33, 9 (1988) 2030.

[20] CHEETHAM, A.D., GONDHALEKAR, A., de HAAS, J.C.M. et al., IAEA-CN-50/I-2-2, 12th IAEA Conf. on Plasma Physics and Controlled Nuclear Fusion (Nice, France) 1988.

x	K	a	b	c	q_{pinch} [kW/m²]	σ [%]
½	0.9±0.1	-0.15±0.05	0.4±0.06	-0.03±0.04	-1.5±1.5	22
²/₃	0.6±0.1	0.3 ±0.09	0.7±0.1	-0.5 ±0.1	-8 ±1.5	23
¾	1.3±0.2	0.5 ±0.1	1.0±0.1	-1.5 ±0.1	-8 ±1.5	22
½ ²/₃ ¾	2.5±0.1	-0.3 ±0.02	-0.1±0.01	0.04±0.02	8 ±1	26

Table I: Values of parameters for the empirical scaling law for χ (Eq.17) obtained from non-linear regression analyses; σ, the mean rms of the relative difference between data and fitted values, represents the scatter.

x	K	a	b	q_{pinch} [kW/m²]	σ [%]
½	3.4±0.2	0.3±0.02	-1.0 ±0.02	17 ±18	23
²/₃	2.8±0.2	0.3±0.02	-0.75±0.05	2.6±2.1	24
¾	3.2±0.15	0.3±0.02	-0.32±0.06	2.1±1.6	27
½ ²/₃ ¾	2.8±0.2	0.4±0.02	-0.9 ±0.01	19 ±18	35

Table II: Values of parameters obtained with the scaling of χ (Eq.18b) based on a gyrokinetic equation.

FIGURE CAPTIONS

Figure 1 Time evolution of the axial electron temperature (ECE) for JET pulse 13428. Application of 10MW of ICRH leads to a sawtooth-free period of duration 2.5 seconds. The errors indicate the transport analysis times for this particular pulse. The labels 1, 2 and 3 refer to times used for grahs in Figure 5.

Figure 2 The similarity of safety factor q_ψ profiles in all analysed pulses is illustrated by four representative q_ψ profiles. These profiles are obtained from equilibrium calculations on four JET pulses each with 7MW of ICRH and plasma currents 2, 2.5, 3, 3.5MA. The abcissae x corresponds to a normalised flux label defined in the text.

Figure 3 The total confined electron energy W_e vs power $P - dW_e/dt$. The symbols label the plasma current as follows: o (2MA), + (2.5MA), (3MA), x (3.5MA). This data is well represented by Eq.(2).

Figure 4 Estimate of fast ion energy W_{ifast} from measurements (Eq.3) vs estimate of W_{ifast} from theory. The latter is $P_{RF}\ \tau_s/2$ where τ_s is given by Eq.(4). The symbols label current as for Figure 3.

Figure 5 Radial profiles of heat flux q(x) given by Eq.(5) calculated from the theory in [14] for JET pulse 13428 (as in Figure 1). The labels 1, 2 and 3 correspond to the time values similarly labelled in Figure 1.

Figure 6 Values of total heat flux q vs $en_e\langle\nabla T_e\rangle$ at the half radius x=½. The symbols label current as in Figure 3. The straight lines are based on linear regression fits and show little variation of the slope. For clarity only 2 and 3.5MA data values are shown. Notice that the heat pinch (offset of straight lines) is very small.

Figure 7 As Figure 6 but data is at ¾ radius. Despite the scatter there is strong and clear variation of the slopes of the straight lines through the data.

Figure 8 The resulting heat diffusivity profile $\chi(x)$ spatially resolved. Symbols label current as in Figure 3. The value near x=0 is obtained from ICRH modulation experiments (5). The result at x=0.4 is derived from heat pulse propagation measurements [18]. The two values with horizontal error bars are determined from pellet injection experiments [20].

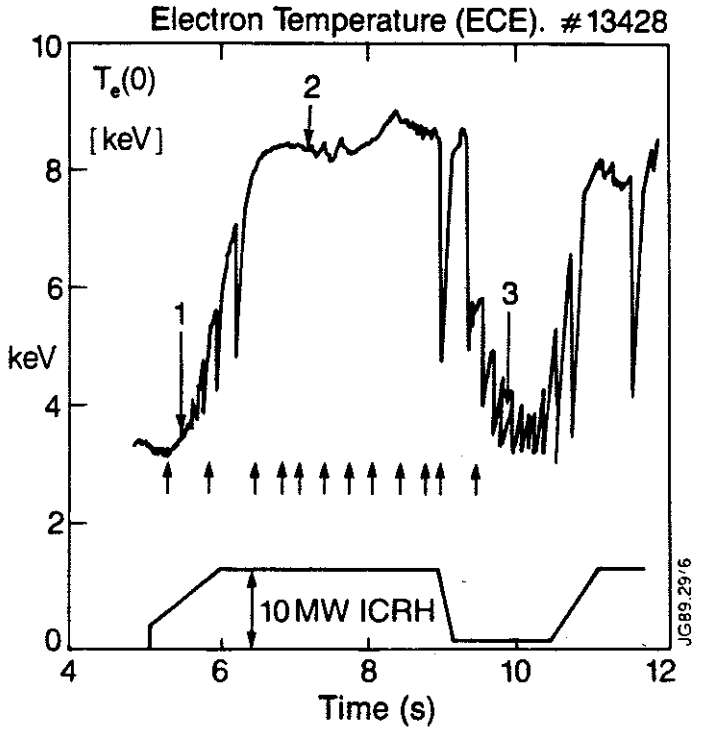

Fig. 1 Time evolution of the axial electron temperature (ECE) for JET pulse 13428. Application of 10 MW of ICRH leads to a sawtooth-free period of duration 2.5 seconds. The errors indicate the transport analysis times for this particular pulse. The labels 1, 2 and 3 refer to times used for graphs in figure 5.

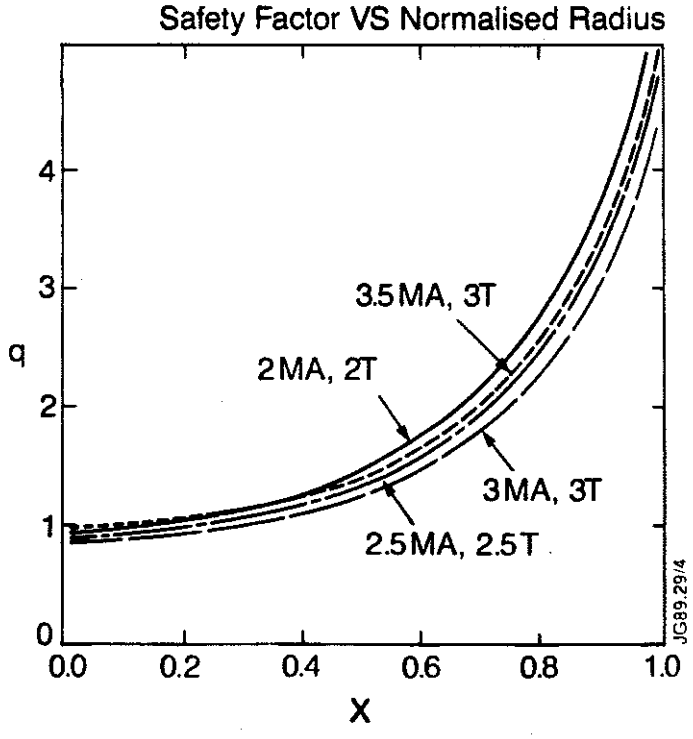

Fig. 2 The similarity of safety factor q_ψ profiles in all analysed pulses is illustrated by four representative q_ψ profiles. These profiles are obtained from equilibrium calculations on four JET pulses each with 7 MW of ICRH and plasma currents 2, 2.5, 3, 3.5 MA. The abcissae x corresponds to a normalised flux label defined in the text.

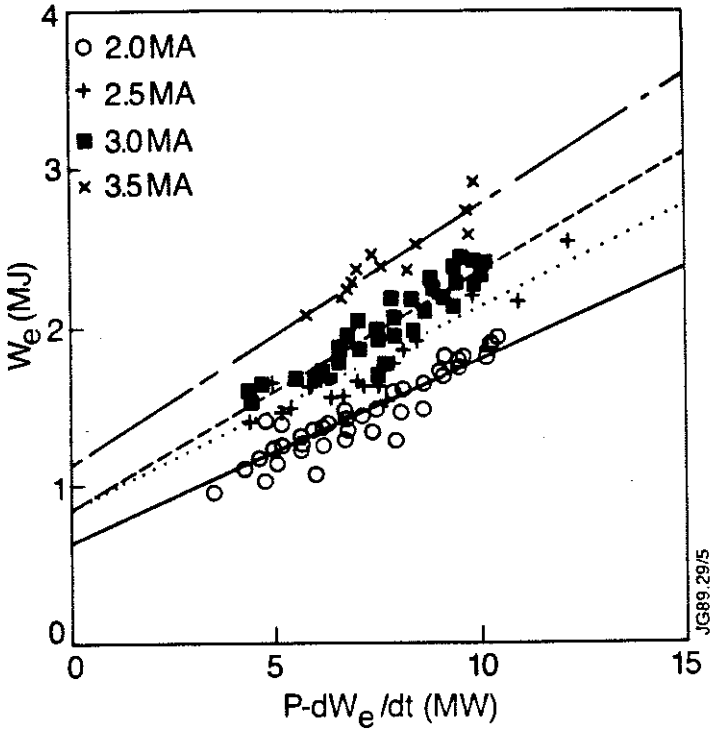

Fig. 3 The total confined electron energy W_e vs power $P-dW_e/dt$. The symbols label the plasma current as follows: 0(2MA), + (2.5MA), (3MA), x(3.5MA). This data is well represented by Eq. (2).

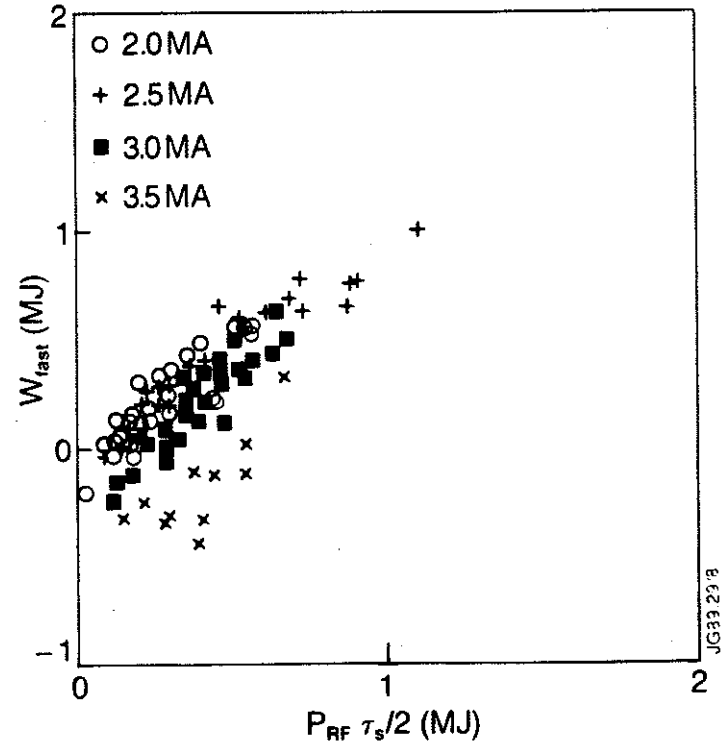

Fig. 4 Estimate of fast ion energy $W_{\perp fast}$ from measurements (Eq.3) vs estimate of $W_{\perp fast}$ from theory. The latter is $P_{RF}\,\tau_s/2$ where τ_s is given by Eq.(4). The symbols label current as for Fig. 3.

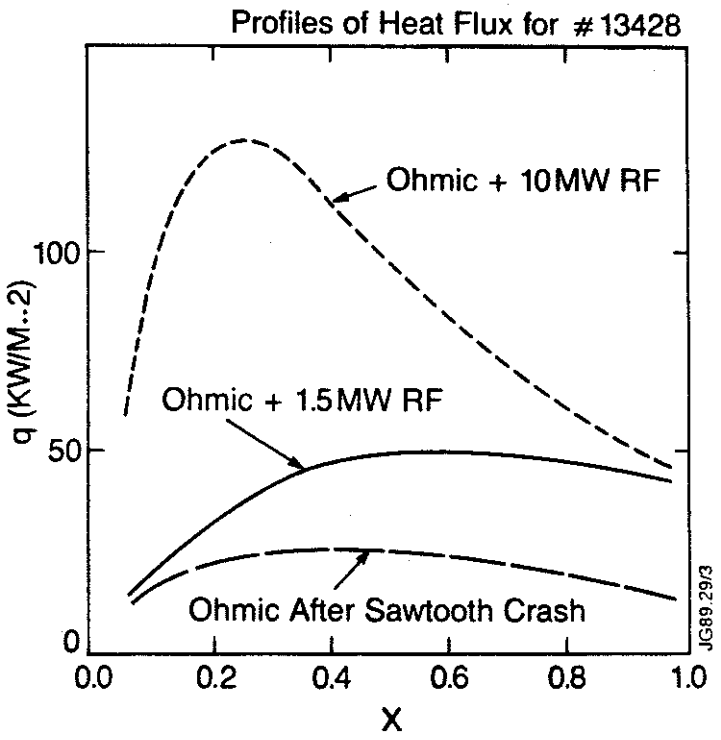

Fig. 5 Radial profiles of heat flux $q(x)$ given by Eq. (5) calculated from the theory in [14] for JET pulse 13482 (as in figure 1). The labels 1, 2 and 3 correspond to the time values similarly labelled in Figure 1.

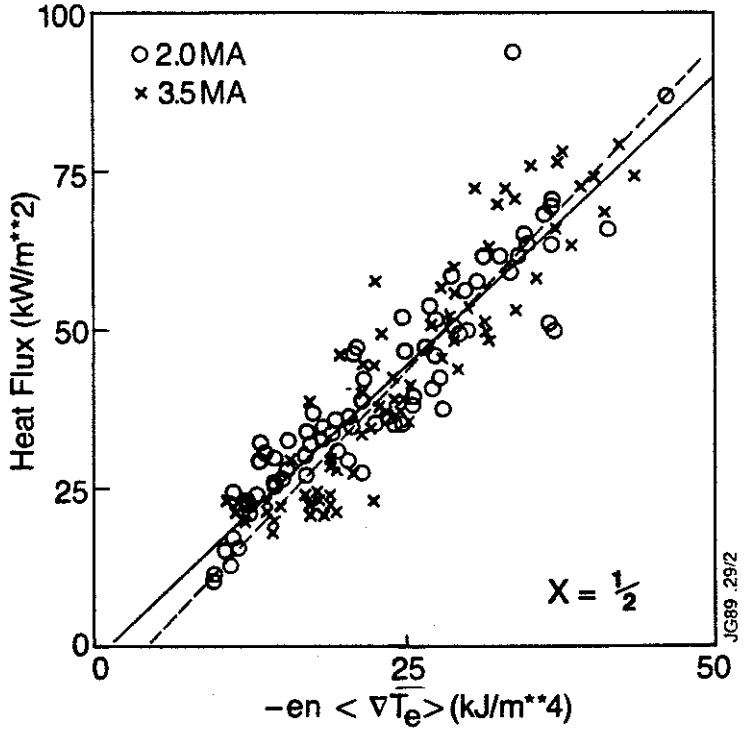

Fig. 6 Values of total heat flux q vs $en_e < \nabla T_e >$ at the half radius x = ½. The symbols label current as in Figure 3. The straight lines are based on linear regression fits and show little variation of the slope. For clarity only 2 and 3.5 MA data values are shown. Notice that the heat pinch (offset of straight lines) is very small.

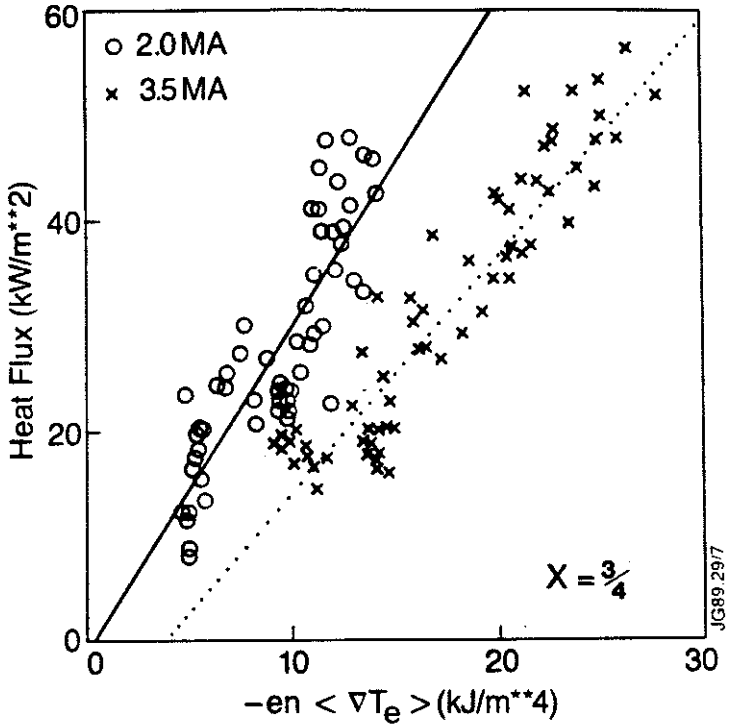

Fig. 7 As Figure 6 but data is at ¾ radius. Despite the scatter there is strong and clear variation of the slopes of the straight lines through the data.

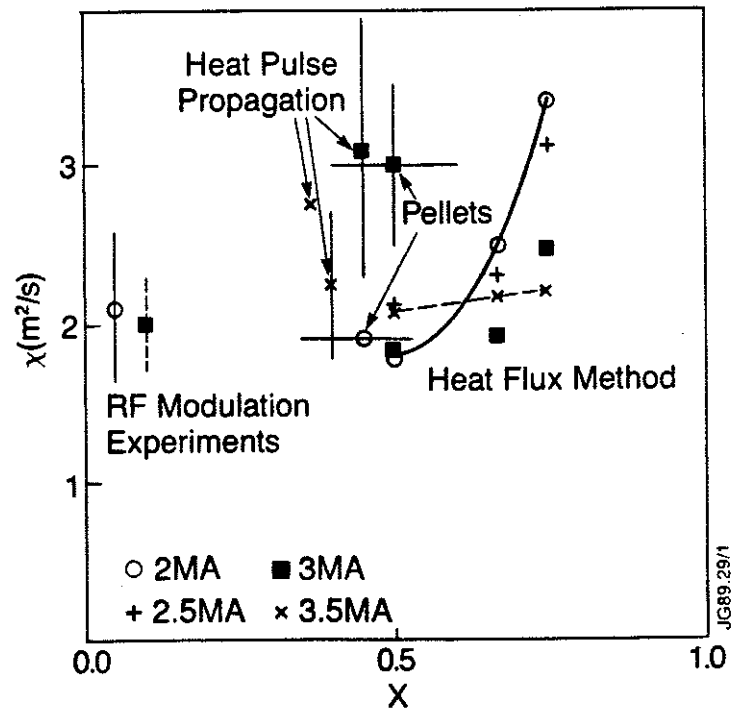

Fig. 8 The resulting heat diffusivity profile $\chi(x)$ spatially resolved. Symbols label current as in Figure 3. The value near $x=0$ is obtained from ICRH modulation experiments (5). The result at $x=0.4$ is derived from heat pulse propagation measurements [18]. The two values with horizontal error bars are determined from pellet injection experiments [20].

APPENDIX 1.

THE JET TEAM

JET Joint Undertaking, Abingdon, Oxon, OX14 3EA, U.K.

J.M.Adams[1], F.Alladio[4], H.Altmann, R.J.Anderson, G.Appruzzese, W.Bailey, B.Balet, D.V.Bartlett, L.R.Baylor[24], K.Behringer, A.C.Bell, P.Bertoldi, E.Bertolini, V.Bhatnagar, R.J.Bickerton, A.Boileau[3], T.Bonicelli, S.J.Booth, G.Bosia, M.Botman, D.Boyd[31], H.Brelen, H.Brinkschulte, M.Brusati, T.Budd, M.Bures, T.Businaro[4], H.Buttgereit, D.Cacaut, C.Caldwell-Nichols, D.J.Campbell, P.Card, J.Carwardine, G.Celentano, P.Chabert[27], C.D.Challis, A.Cheetham, J.Christiansen, C.Christodoulopoulos, P.Chuilon, R.Claesen, S.Clement[30], J.P.Coad, P.Colestock[6], S.Conroy[13], M.Cooke, S.Cooper, J.G.Cordey, W.Core, S.Corti, A.E.Costley, G.Cottrell, M.Cox[7], P.Cripwell[13], F.Crisanti[4], D.Cross, H.de Blank[16], J.de Haas[16], L.de Kock, E.Deksnis, G.B.Denne, G.Deschamps, G.Devillars, K.J.Dietz, J.Dobbing, S.E.Dorling, P.G.Doyle, D.F.Düchs, H.Duquenoy, A.Edwards, J.Ehrenberg[14], T.Elevant[12], W.Engelhardt, S.K.Erents[7], L.G.Eriksonn[5], M.Evrard[2], H.Falter, D.Flory, M.Forrest[7], C.Froger, K.Fullard, M.Gadeberg[11], A.Galetsas, R.Galvao[8], A.Gibson, R.D.Gill, A.Gondhalekar, C.Gordon, G.Gorini, C.Gormezano, N.A.Gottardi, C.Gowers, B.J.Green, F.S.Griph, M.Gryzinski[26], R.Haange, G.Hammett[6], W.Han[9], C.J.Hancock, P.J.Harbour, N.C.Hawkes[7], P.Haynes[7], T.Hellsten, J.L.Hemmerich, R.Hemsworth, R.F.Herzog, K.Hirsch[14], J.Hoekzema, W.A.Houlberg[24], J.How, M.Huart, A.Hubbard, T.P.Hughes[32], M.Hugon, M.Huguet, J.Jacquinot, O.N.Jarvis, T.C.Jernigan[24], E.Joffrin, E.M.Jones, L.P.D.F.Jones, T.T.C.Jones, J.Källne, A.Kaye, B.E.Keen, M.Keilhacker, G.J.Kelly, A.Khare[15], S.Knowlton, A.Konstantellos, M.Kovanen[21], P.Kupschus, P.Lallia, J.R.Last, L.Lauro-Taroni, M.Laux[33], K.Lawson[7], E.Lazzaro, M.Lennholm, X.Litaudon, P.Lomas, M.Lorentz-Gottardi[2], C.Lowry, G.Magyar, D.Maisonnier, M.Malacarne, V.Marchese, P.Massmann, L.McCarthy[28], G.McCracken[7], P.Mendonca, P.Meriguet, P.Micozzi[4], S.F.Mills, P.Millward, S.L.Milora[24], A.Moissonnier, P.L.Mondino, D.Moreau[17], P.Morgan, H.Morsi[14], G.Murphy, M.F.Nave, M.Newman, L.Nickesson, P.Nielsen, P.Noll, W.Obert, D.O'Brien, J.O'Rourke, M.G.Pacco-Düchs, M.Pain, S.Papastergiou, D.Pasini[20], M.Paume[27], N.Peacock[7], D.Pearson[13], F.Pegoraro, M.Pick, S.Pitcher[7], J.Plancoulaine, J-P.Poffé, F.Porcelli, R.Prentice, T.Raimondi, J.Ramette[17], J.M.Rax[27], C.Raymond, P-H.Rebut, J.Removille, F.Rimini, D.Robinson[7], A.Rolfe, R.T.Ross, L.Rossi, G.Rupprecht[14], R.Rushton, P.Rutter, H.C.Sack, G.Sadler, N.Salmon[13], H.Salzmann[14], A.Santagiustina, D.Schissel[25], P.H.Schild, M.Schmid, G.Schmidt[6], R.L.Shaw, A.Sibley, R.Simonini, J.Sips[16], P.Smeulders, J.Snipes, S.Sommers, L.Sonnerup, K.Sonnenberg, M.Stamp, P.Stangeby[19], D.Start, C.A.Steed, D.Stork, P.E.Stott, T.E.Stringer, D.Stubberfield, T.Sugie[18], D.Summers, H.Summers[20], J.Taboda-Duarte[22], J.Tagle[30], H.Tamnen, A.Tanga, A.Taroni, C.Tebaldi[23], A.Tesini, P.R.Thomas, E.Thompson, K.Thomsen[11], P.Trevalion, M.Tschudin, B.Tubbing, K.Uchino[29], E.Usselmann, H.van der Beken, M.von Hellermann, T.Wade, C.Walker, B.A.Wallander, M.Walravens, K.Walter, D.Ward, M.L.Watkins, J.Wesson, D.H.Wheeler, J.Wilks, U.Willen[12], D.Wilson, T.Winkel, C.Woodward, M.Wykes, I.D.Young, L.Zannelli, M.Zarnstorff[6], D.Zasche[14], J.W.Zwart.

PERMANENT ADDRESS

1. UKAEA, Harwell, Oxon. UK.
2. EUR-EB Association, LPP-ERM/KMS, B-1040 Brussels, Belgium.
3. Institute National des Récherches Scientifique, Quebec, Canada.
4. ENEA-CENTRO Di Frascati, I-00044 Frascati, Roma, Italy.
5. Chalmers University of Technology, Göteborg, Sweden.
6. Princeton Plasma Physics Laboratory, New Jersey, USA.
7. UKAEA Culham Laboratory, Abingdon, Oxon. UK.
8. Plasma Physics Laboratory, Space Research Institute, Sao José dos Campos, Brazil.
9. Institute of Mathematics, University of Oxford, UK.
10. CRPP/EPFL, 21 Avenue des Bains, CH-1007 Lausanne, Switzerland.
11. Risø National Laboratory, DK-4000 Roskilde, Denmark.
12. Swedish Energy Research Commission, S-10072 Stockholm, Sweden.
13. Imperial College of Science and Technology, University of London, UK.
14. Max Planck Institut für Plasmaphysik, D-8046 Garching bei München, FRG.
15. Institute for Plasma Research, Gandhinagar Bhat Gujat, India.
16. FOM Instituut voor Plasmafysica, 3430 Be Nieuwegein, The Netherlands.
17. Commissiariat à L'Energie Atomique, F-92260 Fontenay-aux-Roses, France.
18. JAERI, Tokai Research Establishment, Tokai-Mura, Naka-Gun, Japan.
19. Institute for Aerospace Studies, University of Toronto, Downsview, Ontario, Canada.
20. University of Strathclyde, Glasgow, G4 ONG, U.K.
21. Nuclear Engineering Laboratory, Lapeenranta University, Finland.
22. JNICT, Lisboa, Portugal.
23. Department of Mathematics, Univeristy of Bologna, Italy.
24. Oak Ridge National Laboratory, Oak Ridge, Tenn., USA.
25. G.A. Technologies, San Diego, California, USA.
26. Institute for Nuclear Studies, Swierk, Poland.
27. Commissiariat à l'Energie Atomique, Cadarache, France.
28. School of Physical Sciences, Flinders University of South Australia, South Australia SO42.
29. Kyushi University, Kasagu Fukuoka, Japan.
30. Centro de Investigaciones Energeticas Medioambientales y Techalogicas, Spain.
31. University of Maryland, College Park, Maryland, USA.
32. University of Essex, Colchester, UK.
33. Akademie de Wissenschaften, Berlin, DDR.

CR 88.49.1A